



Published in final edited form as:

J Mol Biol. 2007 February 16; 366(2): 469–480. doi:10.1016/j.jmb.2006.11.006.

X-Ray Crystal Structure of *Mycobacterium Tuberculosis* β -Ketoacyl Acyl Carrier Protein Synthase II (*mtKasB*)

Sudharsan Sridharan^{1,*}, Lei Wang¹, Alistair K. Brown², Lynn G. Dover², Laurent Kremer³, Gurdyal S. Besra², and James C. Sacchettini¹

¹Department of Biochemistry and Biophysics, Texas A&M University, College Station, TX 77843-2128, USA

²School of Biosciences, University of Birmingham, Edgbaston, Birmingham, B15 2TT, UK

³Université Montpellier II, Case 107, Place Eugène Bataillon, 34095 Montpellier Cedex 05, France

Summary

Mycolic acids are long chain α -alkyl branched, β -hydroxy fatty acids that represent a characteristic component of the *Mycobacterium tuberculosis* cell wall. Through their covalent attachment to peptidoglycan via an arabinogalactan polysaccharide, they provide the basis for an essential outer envelope membrane. Mycobacteria possess two fatty acid synthases (FAS); FAS-I carries out *de novo* synthesis of fatty acids while FAS-II is considered to elongate medium chain length fatty acyl primers to provide long chain (C₅₆) precursors of mycolic acids. Here we report the crystal structure of *Mycobacterium tuberculosis* β -ketoacyl acyl carrier protein synthase (ACP) II *mtKasB*, a mycobacterial elongation condensing enzyme involved in FAS-II. This enzyme, along with the *M. tuberculosis* β -ketoacyl ACP synthase I *mtKasA*, catalyzes the Claisen-type condensation reaction responsible for fatty acyl elongation in FAS-II and are potential targets for development of novel anti-tubercular drugs. The crystal structure refined to 2.4 Å resolution revealed that, like other KAS-II enzymes, *mtKasB* adopts a thiolase fold but contains unique structural features in the capping region that may be crucial to its preference for longer fatty acyl chains than its counterparts from other bacteria. Modeling of *mtKasA* using the *mtKasB* structure as a template predicts the overall structures to be almost identical, but a larger entrance to the active site tunnel is envisaged that might contribute to the greater sensitivity of *mtKasA* to the inhibitor thiolactomycin (TLM). Modeling of TLM binding in *mtKasB* shows that the drug fits the active site poorly and results of enzyme inhibition assays using TLM analogues are wholly consistent with our structural observations. Consequently, the structure described here further highlights the potential of TLM as an anti-tubercular lead compound and will aid further exploration of the TLM scaffold towards the design of novel compounds which inhibit mycobacterial KAS enzymes more effectively.

Keywords

fatty acid biosynthesis; FAS-II; *mtKasB*; thiolactomycin; drug target

Corresponding author: James C. Sacchettini, 2128 TAMU, Department of Biochemistry and Biophysics, Texas A&M University, College Station, TX 77843-2128, USA. Tel: 979-862-7636; FAX: 979-862-7638; E-mail: sacchett@tamu.edu.

*Current address: Department of Biochemistry, University of Cambridge, 80 Tennis Court Road, Cambridge CB2 1GA, United Kingdom.

Publisher's Disclaimer: This is a PDF file of an unedited manuscript that has been accepted for publication. As a service to our customers we are providing this early version of the manuscript. The manuscript will undergo copyediting, typesetting, and review of the resulting proof before it is published in its final citable form. Please note that during the production process errors may be discovered which could affect the content, and all legal disclaimers that apply to the journal pertain.

Introduction

Mycobacterium tuberculosis, the aetiological agent of tuberculosis (TB), causes more human deaths than any other single infectious pathogen, with an estimated 8 million new cases and 2 million fatalities per annum worldwide¹. TB control has been made difficult in recent years by the apparent synergy between AIDS and TB^{2; 3; 4}. In addition, the length and complexity of current TB treatment regimens result in poor patient compliance, a major factor in emergence of multidrug resistant TB (MDR-TB)⁵. Given the multiple problems in fighting TB, effective control of the disease requires the identification of new drug targets and discovery of novel drugs.

M. tuberculosis has an unusually complex and lipid-rich cell wall which is responsible for the pathogen's intrinsic resistance to many common antibiotics⁶. The essentiality of the mycobacterial cell wall to the survival of the pathogen implies that the pathway to its biosynthesis is an attractive target for novel antimycobacterial chemotherapy⁷. The most distinct feature of the mycobacterial cell wall is the presence of the α -alkyl, β -hydroxy fatty acids termed mycolic acids. These are esterified to the non-reducing termini of the arabinogalactan-peptidoglycan cell wall core forming the inner leaflet of the cell wall permeability barrier^{7; 8}. Although the longer meromycolate chain (up to 56 carbon atoms) of the mycolic acids are modified⁹, its length is essentially provided via conventional fatty acid biosynthesis. Upon completion it is condensed with a C24-C26 fatty acid, which provides the α -alkyl branch of the mature mycolic acid^{8; 10; 11}. Mycobacteria are unusual in that they possess both known types of fatty acid synthase (FAS)⁹; a mammalian-type FAS-I, which carries all of the necessary enzymatic activities and carrier functions on a single polypeptide¹², and a bacterial type FAS-II, in which separate enzymes interact with a discrete acyl carrier protein (ACP) that carries the growing fatty acyl chain between their active sites¹³. In mycobacteria and related genera, FAS-I conducts the *de novo* synthesis of intermediate length (principally C16 and C24) fatty acids. Mycobacterial FAS-II, however, is incapable of *de novo* fatty acid synthesis^{14; 15; 16; 17; 18}. Its ability to elongate C14- and C16-CoA primers has been demonstrated^{10; 18; 19; 20; 21} and current hypotheses suggest that FAS-I products are elongated via FAS-II to form meromycolates⁸.

In both FAS-I and FAS-II, fatty acyl elongation is initiated by a condensation reaction in which malonyl-ACP is decarboxylated and the resulting carbanion attacks an enzyme-linked acyl thioester derived from an acyl-CoA primer^{10; 12; 19}. In FAS-II the initial condensation reaction is carried out by β -ketoacyl ACP synthase (KAS)-III, also referred to as FabH²², however subsequent FAS-II cycles are initiated by acyl-ACP primed β -ketoacyl ACP synthases, KAS-I and KAS-II (KasA and KasB respectively in *M. tuberculosis*, FabB and FabF respectively in *E. coli*)^{10; 16; 22; 23}.

In *E. coli*, the temperature dependent regulation of fatty acid composition is modulated through KAS-II (FabF)^{24; 25}. *E. coli* mutants which lack KAS-II activity are deficient in elongation of palmitoleate to *cis*-vaccenate but show normal growth characteristics under standard culture conditions^{24; 26; 27}. Overexpression of *mtkasB* produced longer chain polyunsaturated hydrocarbons averaging 54 carbons in length²⁸. *M. marinum kasB* mutants grew poorly in macrophages and showed an altered mycolate profile and cell wall permeability²⁹. These results suggest the importance of KasB in mycobacteria and show that it represents an attractive target for novel drug development against *M. tuberculosis*. Thiolactomycin (TLM) has been shown to be an inhibitor of mycobacterial β -ketoacyl ACP synthases^{10; 20; 23} and hence acts as a potent anti-tuberculous agent by inhibiting both fatty acid and mycolic acid biosynthesis¹⁸.

In this work, the X-ray crystal structure of *mtKasB* has been determined using the molecular replacement method. The structure has been described and shows distinct features when compared to other known KAS-II structures^{30; 31; 32; 33}. To gain further knowledge of possible interactions between TLM and *mtKasB*, modeling of the complex has been attempted based on the known crystal structure of a TLM complex with KAS-I (*ecFabB*). The sequences of *mtKasA* and *mtKasB* are 69.5 % identical allowing the modeling of the structure of *mtKasA* based on *mtKasB* and thus comparisons with the mycobacterial KAS-I.

Results and discussion

Quality of the model

The *mtKasB* structure has been solved using a molecular replacement strategy to a resolution of 2.4 Å. The final model has been refined to twinned R/R-free of 23.6%/18.1%. The model consists of two molecules of *mtKasB* and 229 water molecules per asymmetric unit. The electron density was clear for the both molecules in the asymmetric unit except a stretch of residues 128 to 138 and the sidechains of residues 38, 48, 51, 55, 78, 144 and 213 of chain A and the stretch of residues 50 to 58 and 130 to 138 and the sidechains of residues 73, 121, 123, 203, 211, 212 and 213 of chain B. Although C16-CoA was present in the crystallization drop, electron density for the substrate was not observed consistent with *mtKasB* being an acyl-ACP-primed KAS-II. Data collection and refinement statistics are given in Table 1.

Subunit structure

mtKasB shows a homodimeric assembly in the crystal structure. Each subunit has a conserved thiolase fold³⁴ with a five layered $\alpha\beta\alpha\beta\alpha$ core structure similar to the structures of other elongation β -ketoacyl ACP synthases^{30; 31; 32; 33; 35} as shown by structural alignments of the elongation condensing enzymes (Figures 1 and 2). Each subunit is composed of 12 α helices and 15 β strands. The subunit structure consists of two domains – one defining the highly-structured core and the other forming a capping region. Residues 1-260 and 261-415 form topologically equivalent N- and C-terminal $\beta\alpha\beta\alpha\beta\beta$ motifs. The secondary structural elements of the two substructures contribute to similar parts of the core region. This structural aspect suggests that these parts might have arisen as a result of gene duplication although the sequence identity between these parts is only 7%. Although the N-term substructure is more than 100 residues longer than the C-term substructure, the motifs can be superposed with a rmsd of 1.99 Å over 80 C α atoms. The two substructures have different number of insertions between the helices and strand forming the core. The capping region is primarily composed of some of these additional helical segments (α 4, α 6, α 7 and α 10).

Structure of Dimer

The homodimer observed in the asymmetric unit is the functional assembly of this enzyme, based on the similarity to the *E. coli* FabF dimer that has been shown to be dimeric both in solution and in the crystal structure^{30; 36}. In the crystal structure the two subunits are related by a pseudo-two-fold axis (Figure 1). The solvent accessible surface area buried by the dimer is about 6433 Å², 17.7% of the entire surface area of the dimer. Extensive interactions are formed between the subunits and these involve elements from both the core region and the additional elements that are not part of the core. Strand β 5 of the subunits come together in the center of the dimer assembly effectively extending one of the core β -sheets to a 10-stranded twisted β -sheet. The insertion between β 4 and α 8 of the N-term substructure contains the additional elements α 6 and α 7. These elements contribute significantly to both the formation of the dimer and the channel leading to the active site. The residues Ala116, Leu119, Val120 and Tyr123 of α 6 of the capping region contribute significantly to the van der Waals interactions with the helical counterpart from the partner subunit. The residues of the helix α 7 from one subunit line the channel leading to the active site of the partner subunit. Other

interactions contributing to the dimer formation include van der Waals interactions between residues that form the loop regions between $\beta 5$ and $\beta 6$ which includes $\alpha 6$ and $\alpha 7$, between $\beta 10$ and $\alpha 12$ and the helix $\alpha 10$.

Architecture of the active site

The Cys-His-His active site triad is located approximately 15 Å from the surface of the enzyme at the bottom of a molecular tunnel lined by primarily hydrophobic groups from the protein. The mouth of this tunnel measures about 12 Å at its widest part. The residues Phe237, Pro280, Thr313, Thr315, and Phe405 lining the tunnel are conserved in the four other KAS-II structures determined to date (*Synechocystis sp.*, 1E5M³¹; *Thermus thermophilus*, 1J3N³³; *Streptococcus pneumoniae*, 1OX0³² and *E. coli* 1KAS³⁰) and *A. thaliana* mitochondrial KAS (1W0I37).

Alignment of the available structures of the elongation condensing enzymes clearly indicates that the residues Cys170, His311 and His346 of *mtKasB* are highly conserved and positioned appropriately to function as the catalytic residues. Biochemical and mutagenesis studies of condensing enzymes^{38; 39; 40; 41} also show that these residues are the catalytic residues. Cys170 is located at the N-terminus of helix $\alpha 9$ similar to other KAS-II structures. This location has been proposed to promote activation of its sulfhydryl group. Currently, it is accepted that the dipole moment of this helix enhances the nucleophilicity of the sulfur atom by lowering its pKa⁴². In subunit A a water molecule (Wat4) is hydrogen bonded to the backbone carbonyl oxygens of Cys170 (2.7 Å) and Val348 (2.5 Å) (Figure 3a). Wat4 is also within hydrogen-bonding distance from the backbone carbonyl oxygen of Gly349 (2.8 Å) and backbone amide nitrogens of Ser172 (3.5 Å) Gly173 (2.9 Å), and Gly352 (3.0 Å). A water molecule is conserved in this position in *S. pneumoniae*, *T. thermophilus* and *Synechocystis sp.* KAS-II, apo and acyl-bound *ecFabB* (KAS-I) structures (1DD8³⁵ and 1EK4⁴³ respectively) and *A. thaliana* mitochondrial KAS³⁷ suggesting that it may play a structural role such as orienting or maintaining the position of Cys170 in the active site. Incidentally, this water molecule is seen only in subunit A of *mtKasB* and not in subunit B.

Interestingly, His311 and Ala312 were found to be in two different conformations in subunits A and B of *mtKasB* (Figure 3b). Ala312 is unique to *mtKasB* with a glycine occupying the position in the other KAS-II structures. His311 has phi/psi values of $-104.6^\circ/55.0^\circ$ in subunit A and $-86.4^\circ/-13.2^\circ$ in subunit B. Similarly, Ala312 has phi/psi values of $-91.9^\circ/118.3^\circ$ in subunit A and $-30.6^\circ/116.3^\circ$ in subunit B. Comparison of the environment around His311 in the two subunits showed that the difference in the Ala312 conformations is caused by a change in the conformation of Lys341. The conserved Lys341/Glu355 pair is assumed to control the electronic state of His311^{32; 42}. Despite the differing backbone conformations, the N δ of His311 interacts with Lys341 in both the subunits (2.5 Å and 3.4 Å in subunits A and B respectively). Hence, this change in the backbone conformation might not affect the catalytic role of His311. The Lys341-Glu355 salt-bridge interaction is not seen in subunit A of *mtKasB* (N ζ of Lys341 is at distances of 3.8 Å and 3.4 Å from the sidechain carboxylate oxygens of Glu355).

There is also significant difference in orientation of the imidazole ring of the other catalytic histidine residue His346 in the two subunits of *mtKasB*. The plane of the ring in subunit B is about 50° rotated about the C β -C γ bond from that seen in subunit A. Also there are variations in the orientation of the imidazole plane when comparing *mtKasB* and other KAS-II structures (for eg. rotations of about 75° in the *S. pneumoniae* KAS-II structure and about 45° in the *T. thermophilus* structure when comparing with the orientation in subunit A). In all the other KAS-II structures, N ϵ of this His residue interacts with the sulfur of the catalytic Cys residue with an average distance of 3.27 Å between these two atoms. However, in *mtKasB* it is farther away and does not interact with the sulfur (3.6 Å in subunit A and 4.0 Å in subunit B). N δ of

His346 is hydrogen bonded to the backbone amide of the conserved Leu348 in *mtKasB* hence orienting the sidechain so that the N ϵ points toward the active site.

The role of the conserved Lys341 in the catalysis of the KAS enzymes has been analyzed by biochemical and structural studies^{44; 45}. Based on the biochemical studies it was suggested that the interaction between Lys341 and His311 may not be structural in character and that Lys341 may play a more important role in the transacylation half reaction than in the decarboxylation half reaction of the catalysis of the KAS enzymes with Cys-His-His catalytic triad. In this work, we observed different conformations of the His311 and Ala312 due to slight changes in the Lys341 sidechain conformation in *mtKasB*. Wang et al observed significant conformational changes of the catalytic histidines and lack of plastensimycin binding to *ecFabF* (KAS-II) Lys335Ala mutant. These observations suggest that a structural role for this conserved at this position cannot be ruled out. It now seems clear that the conserved lysine plays a critical stereochemical role in orienting the sidechain of the other catalytic histidine His346⁴⁴.

Comparison of KAS II structures

Alignment of *mtKasB*, KAS-I/II, and *A. thaliana* mitochondrial KAS structures revealed interesting structural rearrangements of the capping region of *mtKasB* (rmsd of alignments are given in the legend to Figure 2). Most of the deviations are seen in the insertion segments and the capping region. There is significant rearrangement of the segment containing the helices $\alpha 6$, $\alpha 7$ and $\alpha 10$, all of which are part of the capping region. The $\alpha 6$ helices of the partner subunits contribute to the dimer interface in all of the structures. Analysis of crystal packing of *mtKasB* dimers showed that $\alpha 4$ of subunit B of a dimer lies approximately parallel to $\alpha 6$ of subunit A and prevents a closer approach of $\alpha 6$ of partner subunits in a symmetry-related dimer. This kind of crystal packing is not observed in any of the other KAS-I/II structures.

The apparent rearrangement of the $\alpha 10$ of *mtKasB* involves a shift along its axis towards the surface of the protein. *mtKasB* has a unique Arg residue at position 200 in the short 4-residue stretch connecting $\beta 6$ and $\alpha 10$. Ser or Ala is found at the equivalent position in other KAS-II structures. These shorter sidechains point toward the acyl-binding channels of the corresponding KAS-II structures. The long Arg sidechain in *mtKasB* forces this residue to take a β -conformation exposing the sidechain to solvent. *mtKasB* also has an Ala at position 203 compared to a conserved Pro at the equivalent position in all the other KAS-II structures. A further analysis of $\alpha 10$ showed that the expected backbone hydrogen bonds of an α -helix are formed only in the segment between residues 203 and 210 and not seen in that between residues 207 and 213 in *mtKasB*. The electron density for the residues of $\alpha 10$ of *mtKasB* is clear and thus the elongation of this helix cannot be attributed to errors in building the structural model. Thus, the unique Arg200 residue and the observed hydrogen bonding pattern might explain the difference in arrangement of $\alpha 10$ in *mtKasB* compared to that in other KAS-II structures. Arg213 located at the loop following $\alpha 10$ is one of the residues at the mouth of the active site tunnel. The unique arrangement of $\alpha 10$ described above “pushes” the loop containing Arg213 further towards the surface of the molecule. This makes the mouth of the active site tunnel appear constricted in *mtKasB* in comparison with the other KAS-I/II structures.

It should be noted that $\alpha 10$ spans both the active site tunnel and the acyl binding channel thus forming a structural link between these two cavities. Hence any change in its structure could affect both the channels at the same time. *mtKasB* elongates acyl chains longer than 16 carbons in length. The distal end of the acyl binding channel defined by the *ecFabB*-acyl intermediate structures is closed by $\alpha 6$. Hence, it is intriguing how longer acyl chains could be accommodated in *mtKasB* in this short channel. Attempts to model a C12 acyl chain in the defined channel in *mtKasB* shows that it is not of sufficient length to accommodate longer acyl chains.

Acyl binding channel

The acyl binding channel of elongation condensing enzymes was defined with the structure of the KAS-I (*ecFabB*)-C12/C10 complexes (1EK4/1F91)⁴³. Comparison of KAS-I/II structures clearly indicates that Gly114, Ala169, Phe209 and Phe405 lining the channel are conserved. Gly114 of *mtKasB* appears to be conserved in its position as a bigger sidechain cannot be accommodated in the space available. It is clear that the phenyl ring of Phe405 (Phe392 in 1EK4) has to be rotated about the CB-CG bond in order to accommodate the head part of acyl chains. Alignment of 1EK4 and *mtKasB* structures also showed that the β -turn between the strands β 12 and β 13 which contains Phe405 has shifted by about 2 Å, in turn moving the sidechain of this residue towards the active site tunnel. As a consequence, the active site tunnel in *mtKasB* appears more occluded than in the *ecFabB*-acyl intermediate. In the acyl-bound structure, the backbone amide nitrogens of Phe405 and Ala169 (Ala162 in 1EK4) interact with the oxo-group of the acyl chain. Phe209 is equivalent to Phe201 in 1EK4, the latter dictating the U-shaped conformation of the acyl chain in the acyl-bound structure.

Some interesting differences in the residues lining the acyl binding channel were observed when comparing the structures of *ecFabB*-acyl complex and *mtKasB*. By comparing the structures of complexes of *ecFabB* with C10 and C12 acyl chains (1EK4 and 1FJ1), it was suggested that Glu200 moves to accommodate a longer acyl chain⁴³. In *mtKasB*, the equivalent residue is Gly208 and in the other KAS-II structures, it is a glycine or an alanine. Gln113 in *ecFabB* was found to be in different conformations in the A and B subunits of the structure and the electron density for this residue was well-defined in the complex structure in comparison with the apoenzyme. The sidechain of Gln113 also interacts with the backbone carbonyl group of Gly107 in subunit A. In *mtKasB*, Gln113 is substituted by Leu121 and Gly107 by Leu115. In other KAS-II structures, Ile is found in the place of Gly107 of *ecFabB*. It is seen that the substitution of a Gly107 in *ecFabB* with a longer side chain in KAS-II necessitates a compensatory change in the residues equivalent to Met197 of *ecFabB* to one having a smaller sidechain to avoid a clash between the sidechains in these positions. Hence, in *mtKasB* Met197 is substituted by Pro205 and by Ser, Gly or Ala in the other KAS-II structures. In *ecFabB*, Met197A along with Met138B delineate opposite sides of the acyl binding channel. The latter residue is conserved between *ecFabB* and *mtKasB* but substituted by Ile or Leu in the other KAS-II structures. It should be noted that Pro205, Gly208 and Phe209 of *mtKasB* are located in α 10. These substitutions may reflect the necessary changes required to bind substrates specific to the KAS-II enzymes of different organisms.

The structures of *ecFabB*/F-cerulenin complexes^{46; 47} were also compared with *mtKasB* structure. It is clear from this comparison that Leu115 of *mtKasB* has to be reoriented for CER binding. Olsen et al. observed that the equivalent residue Ile154 in *A. thaliana* mitochondrial KAS would require a similar reorientation to facilitate CER binding³⁷. The structural alignment also clearly shows that Tyr144B of *mtKasB* (Ile183 in *A. thaliana* mitochondrial KAS, Ala137 in *ecFabB* and Thr137 in *ecFabF*) will not allow the orientation of CER seen in the above complexes in *mtKasB*. The energetic barrier to reorient Tyr144B in *mtKasB* to allow a similar CER binding mode as seen in the complexes is expected to be high. Hence we predict that beyond the C7 position CER in *mtKasB* would proceed in a direction different from that seen in the above complexes.

Modeling of *mtKasB*-TLM complex

TLM is a natural product that reversibly inhibits β -ketoacyl ACP synthases. The structure of an *ecFabB*-TLM complex⁴⁶ (PDB code: 1FJ4) has been determined and shows the mechanism of inhibition of this KAS-I enzyme. Although TLM is a poor inhibitor of condensing enzymes, it provides an avenue for rational design of analogues that could be better inhibitors of this class of enzyme. Crystallization of an *mtKasB*-TLM complex was attempted towards this end.

The crystals did not diffract well enough to get useful data required to determine the structure of the complex, hence, modeling of TLM in the *mtKasB* structure was performed with the knowledge of *ecFabB*-TLM complex structure. Energy minimization was done using the program Sybyl and the Discover module of the program package Insight 2000.

The structural model shows that the isoprenoid branch of TLM is sandwiched between the peptide bonds 279-280 and 405-406 similar to that in the *ecFabB*-TLM structure (Figure 4). The model also shows that the active site tunnel in the model is significantly constricted in comparison with that in the *ecFabB*-TLM structure. The model suggests that the β -turn between β 12 and β 13 and the loop connecting β 8 and α 12 might have to undergo significant rearrangements to create an appropriate binding pocket for the TLM. This is in contrast to the *ecFabB*-TLM complex structure where only minimal distortion is required to fit the TLM⁴⁶. The movement of the main chain in the segment of residues from 403 to 409 spanning β 12, β 13 and the β 12- β 13 turn results in partial stacking of the phenyl ring of Phe405 with the thiolcatone ring of TLM (Figure 4). The distortion in the loop formed by residues 272-286 between β 8 and α 12 is partly due to a two residue (Pro282-Asn283) insertion in *mtKasB* in comparison with the loop in *ecFabB* and moves Pro280 to the appropriate position for TLM binding. This two residue insertion occurs in all the other KAS-II structures and *A. thaliana* mitochondrial KAS (Figure 2). It is also seen from the model that the conserved Asp273 in *mtKasB* has to swing away from its position in the apo structure to avoid a clash with the isoprenoid moiety of TLM (Figure 4)

Kremer et al. demonstrated that hydrophobic chain substituents at the C5 position with varying chain length and saturation showed better *in vivo* inhibition activity than TLM²⁰. In contrast, Kim et al.⁴⁸ reported that their studies revealed very little tolerance for substitution at C5 of TLM in assays of condensing enzymes derived from both *E. coli* and *M. tuberculosis*. The significant modifications that seem to be required to the TLM binding site in *mtKasB* as suggested above by our model may explain the high IC₅₀ values reported for TLM and its analogues^{23, 48}.

Modeling of *mtKasA* structure

The high sequence identity between *mtKasB* and *mtKasA* has allowed modeling of the structure of the latter using the *mtKasB* structure determined in this work as a template and as expected, the two structures are almost identical (rmsd of 0.6 Å). The positions of the catalytic site residues of *mtKasA* (Cys167, His307 and His341) and the active site environment are conserved. The Glu355/Lys341 interaction of *mtKasB* is also conserved in *mtKasA* (Glu350/Lys336). The residues of α 6 and α 10 and those lining the acyl binding channel are mostly conserved in the *mtKasA* model.

The residues lining the active site tunnel are also conserved in the two structures and hence the conservation of the hydrophobic nature of the tunnel in *mtKasA*. Superposition of the *mtKasA* model over the *mtKasB* structure shows that the loop following α 6 is shorter in *mtKasA* than in *mtKasB*. In *mtKasA*, a segment of this loop has the sequence 209MRAMST214 whereas in *mtKasB* the sequence is 212MRIVMST218. In *mtKasB* Ile214, Val215 and Phe239 form a hydrophobic core in the active site tunnel (Figure 5). The substitution of 214IV215 of *mtKasB* by single residue (Ala211) in *mtKasA* results in loss of this hydrophobic core in the latter structure.

Interestingly, IC₅₀ of TLM for *mtKasA* is lower than that for *mtKasB* (20 μ M vs. 90 μ M)²³. Kim et al reported IC₅₀'s of two TLM analogues for *mtKasA* that are lower (8 and 16 fold) than that for *mtKasB*⁴⁸. The MIC of TLM for *M. bovis* BCG strain overexpressing *mtKasA* is lower than that for *mtKasB* (80 μ g/mL vs 100 μ g/mL)²⁰. It would be interesting to investigate

if an increased accessibility resulting from a more open active site tunnel in *mtKasA* as consequence of the shorter loop could account at least partly for these lower values.

Synthesis of TLM analogues and structural and biochemical studies will be required to determine structure activity relationships that could be used in further steps of development of inhibitors of *mtKasB* and *mtKasA*. In this regard, IC₅₀ values against *mtKasA* were higher than TLM for analogues (Table 2) **1** (63 μM), **2** (86 μM), **3** (46 μM) and **4** (66 μM) prepared prior to our structural insight into *mtKasB* and *mtKasA*. Analogues **1-4** also possessed IC₅₀ values greater than 150 μM against *mtKasB*. Although, compound **3** possessed a weaker IC₅₀ value against *mtKasA*, it is much more potent *in vivo* possessing a minimum inhibitory concentration (MIC) of 34 μM, in comparison to TLM, which possessed an MIC value of 142 μM against *Mycobacterium bovis* BCG. These results suggest that analogues with improved activities may now be synthesized in a more rationale way aided by the use of the crystal structure of *mtKasB* and modelling studies of *mtKasA* presented in this current report.

Methods

Cloning, overexpression and purification of *mtKasB*

The *mtkasB* gene (*Rv2246*) was cloned from *M. tuberculosis* H37Rv genomic DNA using the upstream primer 5'-aagaagac**atatg**gttaccgggaaagccttccc-3' with a NdeI restriction site (bold letters) and the downstream primer 5'-aag**ctcgag**tcagtagctccgaagcgcattgc-3' with a XhoI restriction site. The amplified product was then digested with the restriction enzymes and ligated with similarly cut pET28b plasmid DNA (Novagen) to form pET28-*mtkasB*; the construct was verified by nucleotide sequencing. For overexpression of *mtkasB*, Rosetta (DE3) cells (Novagen) were transformed with pET28-*mtkasB*. Transformants were selected on Luria-Bertani (LB) agar medium containing kanamycin (50 μg/mL) and chloramphenicol (34 μg/mL) at 37° C. A single colony was picked and used to inoculate 5 mL of LB medium containing 50 μg/mL kanamycin and 34 μg/mL chloramphenicol. This culture was grown to an OD_{600nm} of 0.6 Units at 37° C and used to inoculate a 100 mL starter culture. This starter culture was grown to an OD_{600nm} of 0.6 Units at 37° C and used to inoculate 4 liters of LB medium. After this culture reached an OD_{600nm} of 0.8 Units, it was cooled to 20° C. IPTG was added to a concentration of 1 mM to induce *mtKasB* overexpression and the medium was further incubated for 12 hrs at 20° C.

The cells were harvested by centrifuging at 3000 × g for 30 minutes and the pelleted cells were resuspended in buffer A (20 mM Tris pH 7.5, 0.5 M NaCl, 2 mM β-mercaptoethanol) at 4° C. DNase I at a final concentration of 10 μg/mL and protease inhibitor cocktail (Calbiochem) were added to the suspension before lysis using a French pressure cell at 1000 psi. The crude lysate was clarified by centrifugation at 10,000 × g for 60 minutes maintaining the temperature at 4° C. The clarified lysate was filtered (0.22 microns) before subsequent chromatographic purification steps performed at 4° C.

mtKasB was purified to near homogeneity using nickel affinity and gel filtration chromatography techniques with performance being monitored using SDS-PAGE. The clarified lysate was passed through the Ni²⁺-charged HiTrap chelating agarose columns equilibrated with buffer A. The columns were washed with 5 column volumes of buffer A to remove unbound and loosely bound contaminant proteins. *mtKasB* bound to the matrix in the columns was eluted using a stepwise gradient of imidazole concentration using 20 mM Tris pH 7.5, 0.5 M NaCl, 2 mM β-mercaptoethanol, 0.5 mM imidazole as buffer B. The bound protein was found to elute with 150 mM imidazole. The eluted protein was dialyzed against gel filtration buffer (20 mM Tris pH 7.5, 10 mM NaCl, 10% glycerol, 1 mM EDTA, 1mM DTT) to remove imidazole. *mtKasB* was concentrated and further purified using a Superdex 200 gel filtration column (Amersham Pharmacia).

mtKasB eluted in two peaks from the gel filtration column. The fractions of the higher molecular weight peak contained a small fraction of *mtKasB* and contaminating proteins and were not used any further. Most of the *mtKasB* eluted in the fractions of the second peak, corresponding to the expected elution volume of *mtKasB* dimer (m.wt. of approximately 88 kDa). These fractions were pooled, concentrated to 30 mg/mL and stored at -80°C in the gel filtration buffer or used directly for crystallization purposes. TLM analogues (Table 2) previously reported by Senior et al.⁴⁹ were assayed against *mtKasB* and *mtKasA* using methods previously described by Schaeffer et al.⁵⁰

Crystallization and data collection

Initial screening for crystallization of *mtKasB* was done using the hanging drop vapor diffusion method. Crystallization conditions obtained commercially from Hampton Research (Crystal Screen and Crystal Screen II) and Emerald Biostructures (Wizard Screens I and II) were screened. Wizard screen II condition 39 (100 mM CAPS pH 10.5, 20 % w/v PEG 8000, 200 mM NaCl) produced crystals that diffracted poorly to 8 Å resolution. Optimization of the above crystallization condition was carried out with additives and detergents (from Hampton research) using sitting drop plates in the presence of C16-CoA. Finally, addition of 5 mM C16-CoA, 0.3 μL Spermine HCl as additive and 0.1 μL Foscholine-9 as detergent with the above crystallization buffer produced crystals that diffracted to 3 Å resolution.

X-ray intensity data was collected at the synchrotron facility at the Center for Advanced Microstructures and Devices (CAMD), Louisiana using a MarCCD system under cryogenic conditions. Several crystals were screened to find one that diffracted better than 3 Å resolution. One of the crystals diffracted to 2.4 Å resolution and was used to collect a total of 180° of data using 1° oscillation range per frame.

Structure determination

The diffraction data was indexed using HKL2000⁵¹ which showed that *mtKasB* crystallized in the space group R3 with unit cell dimensions of $a=b=198.68\text{ \AA}$, $c=71.83\text{ \AA}$, $\alpha=\beta=90^{\circ}$, $\gamma=120^{\circ}$. The data were further integrated and scaled using the program HKL2000. The crystal structure of *mtKasB* was solved using molecular replacement method. First, an initial structural model of *mtKasB* was generated by submitting the protein sequence to and using the first approach mode of the SwissModel software server (<http://swissmodel.expasy.org/SWISS-MODEL.html>)⁵². In this mode, the software automatically chooses the structural templates from the Protein Data Bank (PDB) to build a model for the sequence submitted. This structure was used as the search model to obtain initial phases. Molecular replacement rotation and translation searches to determine the correct orientation of the search model in the unit cell were done using the MolRep program⁵³ of the CCP4 suite⁵⁴. Although a clear solution was obtained, initial electron density maps (2mFo-DFc) obtained after a few cycles of coordinate and B-factor refinement, carried out using the Refmac 55 program of the CCP4 suite, was poor with many discontinuities along the main chain of the electron density and poor or non-existent density for the sidechains of many residues. However, model building using XtalView⁵⁶ was attempted to fit as many residues as possible in the available map. After a few rounds of iterative model building and refinement there was no improvement in the quality of the electron density map. Further, the R-factor/R-free factor remained high at 36%/25% after several steps of refinement without further improvement. At this point, data twinning was suspected and the data was analyzed for twinning, using Yeates' Twinning Server (<http://nihserver.mbi.ucla.edu/Twinning/>)⁵⁷, CCP4, and the Crystallography and NMR System (CNS)⁵⁸ suites. Analysis of these results indicated that the diffraction data was merohedrally twinned with a twin fraction of 41%. When the structure was refined using scripts in the CNS suite that take data twinning into account (the *detwin_partial.inp* script was used which incorporates the twin fraction directly into the

refinement target) the structure and electron density maps improved dramatically, During the final few rounds of model building, water molecules were also added to the model. Iterative refinement and model building yielded the final model of *mtKasB* with an R-factor of 18.1% and an R-free of 23.6%. and good stereo chemistry. The data and structure are deposited in the Protein Data Bank (PDB code 2GP6).

The structural model of *mtKasA* was generated in SwissModel ⁵² using the structure of *mtKasB* as the template. The sequence of *mtKasA* and the structure of *mtKasB* were submitted to the server and the first approach mode was used to generate the *mtKasA* structural model.

ACKNOWLEDGEMENTS

GSB was supported by a Lister-Jenner Institute Research Fellowship and by the Medical Research Council (UK).

REFERENCES

1. Dye C, Scheele S, Dolin P, Pathania V, Raviglione MC. Consensus statement. Global burden of tuberculosis: estimated incidence, prevalence, and mortality by country. WHO Global Surveillance and Monitoring Project. *Jama* 1999;282:677–86. [PubMed: 10517722]
2. Wallis RS, Ellner JJ, Shiratsuchi H. Macrophages, mycobacteria and HIV: the role of cytokines in determining mycobacterial virulence and regulating viral replication. *Res Microbiol* 1992;143:398–405. [PubMed: 1455067]
3. Toossi Z, Mayanja-Kizza H, Hirsch CS, Edmonds KL, Spahlinger T, Hom DL, Aung H, Mugenyi P, Ellner JJ, Whalen CW. Impact of tuberculosis (TB) on HIV-1 activity in dually infected patients. *Clin Exp Immunol* 2001;123:233–8. [PubMed: 11207653]
4. Paolo J, William F, Nosanchuk JD. Tuberculosis in New York city: recent lessons and a look ahead. *The Lancet Infectious Diseases* 2004;4:287–293. [PubMed: 15120345]
5. Kaye K, Frieden TR. Tuberculosis control: the relevance of classic principles in an era of acquired immunodeficiency syndrome and multidrug resistance. *Epidemiol Rev* 1996;18:52–63. [PubMed: 8877330]
6. Hong X, Hopfinger AJ. Molecular modeling and simulation of Mycobacterium tuberculosis cell wall permeability. *Biomacromolecules* 2004;5:1066–77. [PubMed: 15132701]
7. Brennan PJ, Nikaido H. The envelope of mycobacteria. *Annu Rev Biochem* 1995;64:29–63. [PubMed: 7574484]
8. Dover LG, Cerdano-Tarraga AM, Pallen MJ, Parkhill J, Besra GS. Comparative cell wall core biosynthesis in the mycolated pathogens, Mycobacterium tuberculosis and Corynebacterium diphtheriae. *FEMS Microbiol Rev* 2004;28:225–50. [PubMed: 15109786]
9. Kremer, L.; Baulard, A.; Besra, GS. Molecular Genetics of Mycobacteria. Hatfull, GF.; Jacobs, WR., Jr., editors. ASM; Washington D.C.: 2000.
10. Kremer L, Dover LG, Carrere S, Nampoothiri KM, Lesjean S, Brown AK, Brennan PJ, Minnikin DE, Loch C, Besra GS. Mycolic acid biosynthesis and enzymic characterization of the beta-ketoacyl-ACP synthase A-condensing enzyme from Mycobacterium tuberculosis. *Biochem J* 2002;364:423–30. [PubMed: 12023885]
11. Portevin D, De Sousa-D'Auria C, Houssin C, Grimaldi C, Chami M, Daffe M, Guilhot C. A polyketide synthase catalyzes the last condensation step of mycolic acid biosynthesis in mycobacteria and related organisms. *Proc Natl Acad Sci U S A* 2004;101:314–9. [PubMed: 14695899]
12. Smith S, Witkowski A, Joshi AK. Structural and functional organization of the animal fatty acid synthase. *Prog Lipid Res* 2003;42:289–317. [PubMed: 12689621]
13. Lu YJ, Zhang YM, Rock CO. Product diversity and regulation of type II fatty acid synthases. *Biochem Cell Biol* 2004;82:145–55. [PubMed: 15052334]
14. Bloch K. Control mechanisms for fatty acid synthesis in Mycobacterium smegmatis. *Adv Enzymol Relat Areas Mol Biol* 1977;45:1–84. [PubMed: 21523]
15. Cole ST, Brosch R, Parkhill J, Garnier T, Churcher C, Harris D, Gordon SV, Eiglmeier K, Gas S, Barry CE 3rd, Tekaia F, Badcock K, Basham D, Brown D, Chillingworth T, Connor R, Davies R,

- Devlin K, Feltwell T, Gentles S, Hamlin N, Holroyd S, Hornsby T, Jagels K, Krogh A, McLean J, Moule S, Murphy L, Oliver K, Osborne J, Quail MA, Rajandream MA, Rogers J, Rutter S, Seeger K, Skelton J, Squares R, Squares S, Sulston JE, Taylor K, Whitehead S, Barrell BG. Deciphering the biology of *Mycobacterium tuberculosis* from the complete genome sequence. *Nature* 1998;393:537–44. [PubMed: 9634230]
16. Mdluli K, Slayden RA, Zhu Y, Ramaswamy S, Pan X, Mead D, Crane DD, Musser JM, Barry CE 3rd. Inhibition of a *Mycobacterium tuberculosis* beta-ketoacyl ACP synthase by isoniazid. *Science* 1998;280:1607–10. [PubMed: 9616124]
 17. Peterson DO, Bloch K. *Mycobacterium smegmatis* fatty acid synthetase. Long chain transacylase chain length specificity. *J Biol Chem* 1977;252:5735–9. [PubMed: 885878]
 18. Slayden RA, Lee RE, Armour JW, Cooper AM, Orme IM, Brennan PJ, Besra GS. Antimycobacterial action of thiolactomycin: an inhibitor of fatty acid and mycolic acid synthesis. *Antimicrob Agents Chemother* 1996;40:2813–9. [PubMed: 9124847]
 19. Choi KH, Kremer L, Besra GS, Rock CO. Identification and substrate specificity of beta -ketoacyl (acyl carrier protein) synthase III (mtFabH) from *Mycobacterium tuberculosis*. *J Biol Chem* 2000;275:28201–7. [PubMed: 10840036]
 20. Kremer L, Douglas JD, Baulard AR, Morehouse C, Guy MR, Alland D, Dover LG, Lakey JH, Jacobs WR Jr, Brennan PJ, Minnikin DE, Besra GS. Thiolactomycin and related analogues as novel anti-mycobacterial agents targeting KasA and KasB condensing enzymes in *Mycobacterium tuberculosis*. *J Biol Chem* 2000;275:16857–64. [PubMed: 10747933]
 21. Brown AK, Sridharan S, Kremer L, Lindenberg S, Dover LG, Sacchettini JC, Besra GS. Probing the mechanism of the *Mycobacterium tuberculosis* beta-ketoacyl-acyl carrier protein synthase III mtFabH: factors influencing catalysis and substrate specificity. *J Biol Chem* 2005;280:32539–47. [PubMed: 16040614]
 22. Heath RJ, Rock CO. The Claisen condensation in biology. *Nat Prod Rep* 2002;19:581–96. [PubMed: 12430724]
 23. Schaeffer ML, Agnihotri G, Volker C, Kallender H, Brennan PJ, Lonsdale JT. Purification and biochemical characterization of the *Mycobacterium tuberculosis* beta-ketoacyl-acyl carrier protein synthases KasA and KasB. *J Biol Chem* 2001;276:47029–37. [PubMed: 11600501]
 24. Garwin JL, Klages AL, Cronan JE Jr. Beta-ketoacyl-acyl carrier protein synthase II of *Escherichia coli*. Evidence for function in the thermal regulation of fatty acid synthesis. *J Biol Chem* 1980;255:3263–5. [PubMed: 6988423]
 25. de Mendoza D, Klages Ulrich A, Cronan JE Jr. Thermal regulation of membrane fluidity in *Escherichia coli*. Effects of overproduction of beta-ketoacyl-acyl carrier protein synthase I. *J Biol Chem* 1983;258:2098–101. [PubMed: 6337151]
 26. Gelmann EP, Cronan JE Jr. Mutant of *Escherichia coli* deficient in the synthesis of cis-vaccenic acid. *J Bacteriol* 1972;112:381–7. [PubMed: 4562402]
 27. Garwin JL, Klages AL, Cronan JE Jr. Structural, enzymatic, and genetic studies of beta-ketoacyl-acyl carrier protein synthases I and II of *Escherichia coli*. *J Biol Chem* 1980;255:11949–56. [PubMed: 7002930]
 28. Slayden RA, Barry CE 3rd. The role of KasA and KasB in the biosynthesis of meromycolic acids and isoniazid resistance in *Mycobacterium tuberculosis*. *Tuberculosis (Edinb)* 2002;82:149–60. [PubMed: 12464486]
 29. Gao LY, Laval F, Lawson EH, Groger RK, Woodruff A, Morisaki JH, Cox JS, Daffe M, Brown EJ. Requirement for kasB in *Mycobacterium* mycolic acid biosynthesis, cell wall impermeability and intracellular survival: implications for therapy. *Mol Microbiol* 2003;49:1547–63. [PubMed: 12950920]
 30. Huang W, Jia J, Edwards P, Dehesh K, Schneider G, Lindqvist Y. Crystal structure of beta-ketoacyl-acyl carrier protein synthase II from *E.coli* reveals the molecular architecture of condensing enzymes. *Embo J* 1998;17:1183–91. [PubMed: 9482715]
 31. Moche M, Dehesh K, Edwards P, Lindqvist Y. The crystal structure of beta-ketoacyl-acyl carrier protein synthase II from *Synechocystis* sp. at 1.54 Å resolution and its relationship to other condensing enzymes. *J Mol Biol* 2001;305:491–503. [PubMed: 11152607]

32. Price AC, Rock CO, White SW. The 1.3-Ångstrom-resolution crystal structure of beta-ketoacyl-acyl carrier protein synthase II from *Streptococcus pneumoniae*. *J Bacteriol* 2003;185:4136–43. [PubMed: 12837788]
33. Bagautdinov B, Miyano M, Tahirov TH. Crystal Structure of 3-Oxoacyl-(Acyl-Carrier Protein) Synthase II from *Thermus Thermophilus*. 2003 to be published
34. Mathieu M, Zeelen JP, Pauptit RA, Erdmann R, Kunau WH, Wierenga RK. The 2.8 Å crystal structure of peroxisomal 3-ketoacyl-CoA thiolase of *Saccharomyces cerevisiae*: a five-layered alpha beta alpha beta alpha structure constructed from two core domains of identical topology. *Structure* 1994;2:797–808. [PubMed: 7812714]
35. Olsen JG, Kadziola A, von Wettstein-Knowles P, Siggaard-Andersen M, Lindquist Y, Larsen S. The X-ray crystal structure of beta-ketoacyl [acyl carrier protein] synthase I. *FEBS Lett* 1999;460:46–52. [PubMed: 10571059]
36. Edwards P, Nelsen JS, Metz JG, Dehesh K. Cloning of the fabF gene in an expression vector and in vitro characterization of recombinant fabF and fabB encoded enzymes from *Escherichia coli*. *FEBS Lett* 1997;402:62–6. [PubMed: 9013860]
37. Olsen JG, Rasmussen AV, von Wettstein-Knowles P, Henriksen A. Structure of the mitochondrial beta-ketoacyl-[acyl carrier protein] synthase from *Arabidopsis* and its role in fatty acid synthesis. *FEBS Lett* 2004;577:170–4. [PubMed: 15527780]
38. Davies C, Heath RJ, White SW, Rock CO. The 1.8 Å crystal structure and active-site architecture of beta-ketoacyl-acyl carrier protein synthase III (FabH) from *Escherichia coli*. *Structure Fold Des* 2000;8:185–95. [PubMed: 10673437]
39. Funabashi H, Kawaguchi A, Tomoda H, Omura S, Okuda S, Iwasaki S. Binding site of cerulenin in fatty acid synthetase. *J Biochem (Tokyo)* 1989;105:751–5. [PubMed: 2666407]
40. Kauppinen S, Siggaard-Andersen M, von Wettstein-Knowles P. beta-Ketoacyl-ACP synthase I of *Escherichia coli*: nucleotide sequence of the fabB gene and identification of the cerulenin binding residue. *Carlsberg Res Commun* 1988;53:357–70. [PubMed: 3076376]
41. McGuire KA, Siggaard-Andersen M, Banger MG, Olsen JG, von Wettstein-Knowles P. beta-Ketoacyl-[acyl carrier protein] synthase I of *Escherichia coli*: aspects of the condensation mechanism revealed by analyses of mutations in the active site pocket. *Biochemistry* 2001;40:9836–45. [PubMed: 11502177]
42. White SW, Zheng J, Zhang YM, Rock. The structural biology of type II fatty acid biosynthesis. *Annu Rev Biochem* 2005;74:791–831. [PubMed: 15952903]
43. Olsen JG, Kadziola A, von Wettstein-Knowles P, Siggaard-Andersen M, Larsen S. Structures of beta-ketoacyl-acyl carrier protein synthase I complexed with fatty acids elucidate its catalytic machinery. *Structure (Camb)* 2001;9:233–43. [PubMed: 11286890]
44. von Wettstein-Knowles P, Olsen JG, McGuire KA, Henriksen A. Fatty acid synthesis. Role of active site histidines and lysine in Cys-His-His-type beta-ketoacyl-acyl carrier protein synthases. *FEBS J* 2006;273:695–710. [PubMed: 16441657]
45. Wang J, Soisson SM, Young K, Shoop W, Kodali S, Galgoci A, Painter R, Parthasarathy G, Tang YS, Cummings R, Ha S, Dorso K, Motyl M, Jayasuriya H, Ondeyka J, Herath K, Zhang C, Hernandez L, Allocco J, Basilio A, Tormo JR, Genilloud O, Vicente F, Pelaez F, Colwell L, Lee SH, Michael B, Felcetto T, Gill C, Silver LL, Hermes JD, Bartizal K, Barrett J, Schmatz D, Becker JW, Cully D, Singh SB. Platensimycin is a selective FabF inhibitor with potent antibiotic properties. *Nature* 2006;441:358–61. [PubMed: 16710421]
46. Price AC, Choi KH, Heath RJ, Li Z, White SW, Rock CO. Inhibition of beta-ketoacyl-acyl carrier protein synthases by thiolactomycin and cerulenin. Structure and mechanism. *J Biol Chem* 2001;276:6551–9. [PubMed: 11050088]
47. Moche M, Schneider G, Edwards P, Dehesh K, Lindqvist Y. Structure of the complex between the antibiotic cerulenin and its target, beta-ketoacyl-acyl carrier protein synthase. *J Biol Chem* 1999;274:6031–4. [PubMed: 10037680]
48. Kim P, Zhang YM, Shenoy G, Nguyen QA, Boshoff HI, Manjunatha UH, Goodwin MB, Lonsdale J, Price AC, Miller DJ, Duncan K, White SW, Rock CO, Barry CE 3rd, Dowd CS. Structure-activity relationships at the 5-position of thiolactomycin: an intact (5R)-isoprene unit is required for activity

- against the condensing enzymes from *Mycobacterium tuberculosis* and *Escherichia coli*. *J Med Chem* 2006;49:159–71. [PubMed: 16392800]
49. Senior SJ, Illarionov PA, Gurcha SS, Campbell IB, Schaeffer ML, Minnikin DE, Besra GS. Biphenyl-based analogues of thiolactomycin, active against *Mycobacterium tuberculosis* mtFabH fatty acid condensing enzyme. *Bioorg Med Chem Lett* 2003;13:3685–8. [PubMed: 14552758]
 50. Schaeffer ML, Carson JD, Kallender H, Lonsdale JT. Development of a scintillation proximity assay for the *Mycobacterium tuberculosis* KasA and KasB enzymes involved in mycolic acid biosynthesis. *Tuberculosis (Edinb)* 2004;84:353–60. [PubMed: 15525558]
 51. Otwinowski, Z.; Minor, W.; Carter, CWJ.; Sweet, RM., editors. *Methods Enzymol.* 276. Academic Press; 1997. Processing of X-ray diffraction data collected in oscillation mode.
 52. Schwede T, Kopp J, Guex N, Peitsch MC. SWISS-MODEL: An automated protein homology-modeling server. *Nucleic Acids Res* 2003;31:3381–5. [PubMed: 12824332]
 53. Vagin AA, Teplyakov A. MOLREP: an automated program for molecular replacement. *J. Appl. Cryst* 1997;30:1022–25.
 54. CCP4. The CCP4 suite: programs for protein crystallography. *Acta Crystallogr D Biol Crystallogr* 1994;50:760–3. [PubMed: 15299374]
 55. Murshudov GN, Vagin AA, Dodson EJ. Refinement of Macromolecular Structures by the Maximum-Likelihood Method. *Acta Crystallogr D Biol Crystallogr* 1997;53:240–55. [PubMed: 15299926]
 56. McRee DE. XtalView/Xfit--A versatile program for manipulating atomic coordinates and electron density. *J Struct Biol* 1999;125:156–65. [PubMed: 10222271]
 57. Yeates TO. Detecting and overcoming crystal twinning. *Methods Enzymol* 1997;276:344–58. [PubMed: 9048378]
 58. Brunger AT, Adams PD, Clore GM, DeLano WL, Gros P, Grosse-Kunstleve RW, Jiang JS, Kuszewski J, Nilges M, Pannu NS, Read RJ, Rice LM, T. S, Warren GL. Crystallography & NMR system: A new software suite for macromolecular structure determination. *Acta Crystallogr D Biol Crystallogr* 1999;54:905–21. [PubMed: 9757107]
 59. Krissinel E, Henrick K. Secondary-structure matching (SSM), a new tool for fast protein structure alignment in three dimensions. *Acta Crystallogr D Biol Crystallogr* 2004;60:2256–68. [PubMed: 15572779]

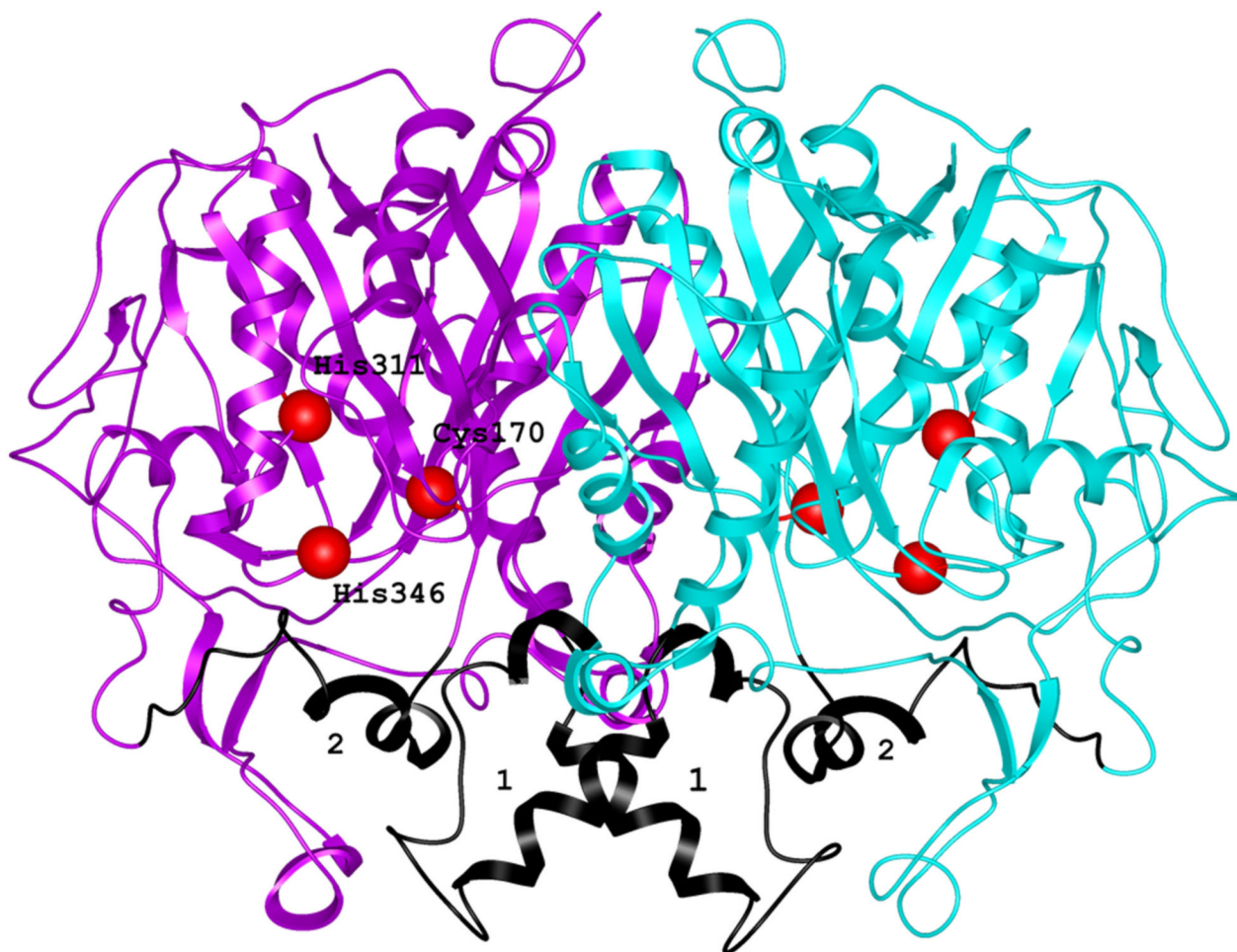


Figure 1. Ribbon representation of *mtKasB* dimer. The two subunits are shown in magenta and cyan. The positions of the active site residues are shown as red spheres and labeled. The segments shown in black and labeled 1 and 2 correspond to the regions showing large deviations when compared to KAS-I/II structures. These segments are also referred to in Figure 2.

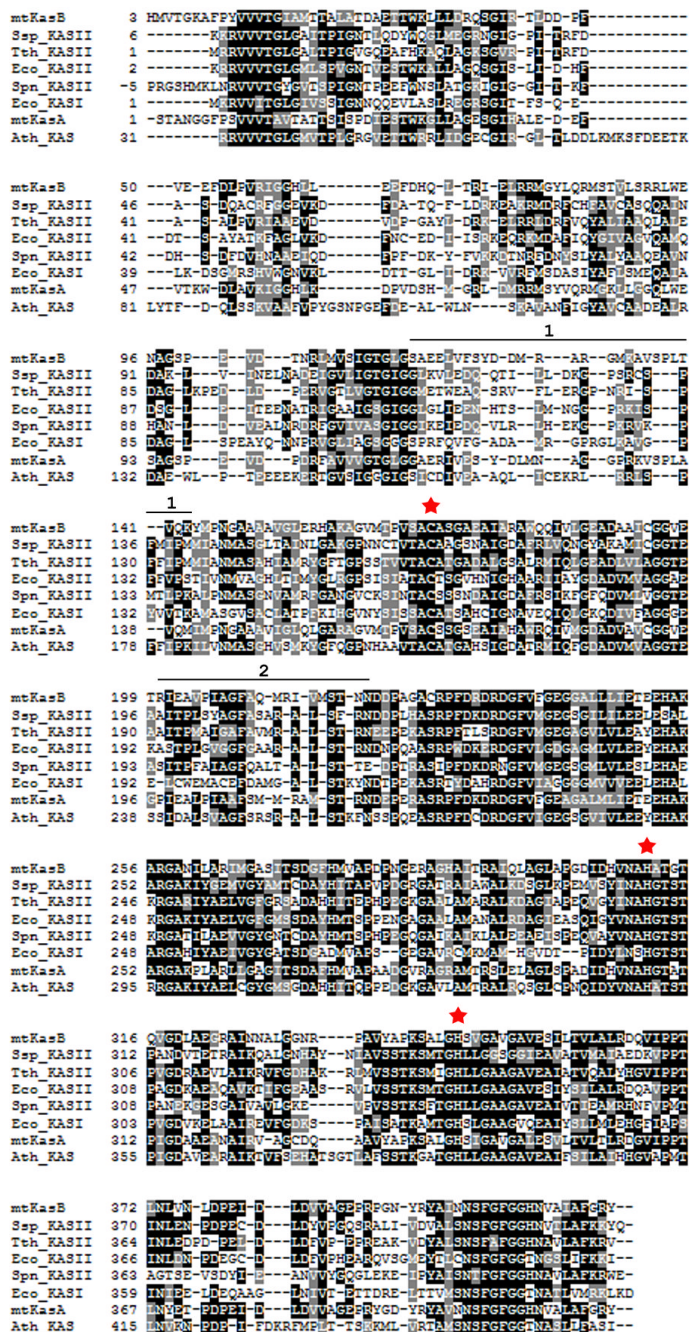


Figure 2. Structure based alignment of KAS-I/II sequences. A structure based alignment was generated for KAS-I/II sequences using Protein structure comparison service SSM at European Bioinformatics institute⁵⁹ (<http://www.ebi.ac.uk/msd-srv/ssm>) and Boxshade (http://www.ch.embnet.org/software/BOX_form.html). The red stars mark the active site residues. The stretches of sequence marked by the black line above the *mtKasB* sequence and labeled 1 and 2 refer to the segments colored in black in Figure 1. *Ssp_KASII* - *Synechocystis sp.* KAS II (PDB code of the structure used in alignment: 1E5M, rmsd of alignment with *mtKasB* reported by the SSM service: 1.6 Å), *Tth_KASII* - *T. thermophilus* KAS II (1J3N, 1.5 Å), *Eco_KASII* - *E.coli* FabF (1KAS, 1.6 Å), *Spn_KASII* - *S. pneumoniae* KAS II (1OX0, 1.7

Å), Eco_KASI - *E.coli* FabB (1DD8, 1.7 Å), mtKasA - *M. tuberculosis* KasA (0.6 Å), Ath_KAS - *A. thaliana* mitochondrial KAS (1W0I, 1.7 Å).

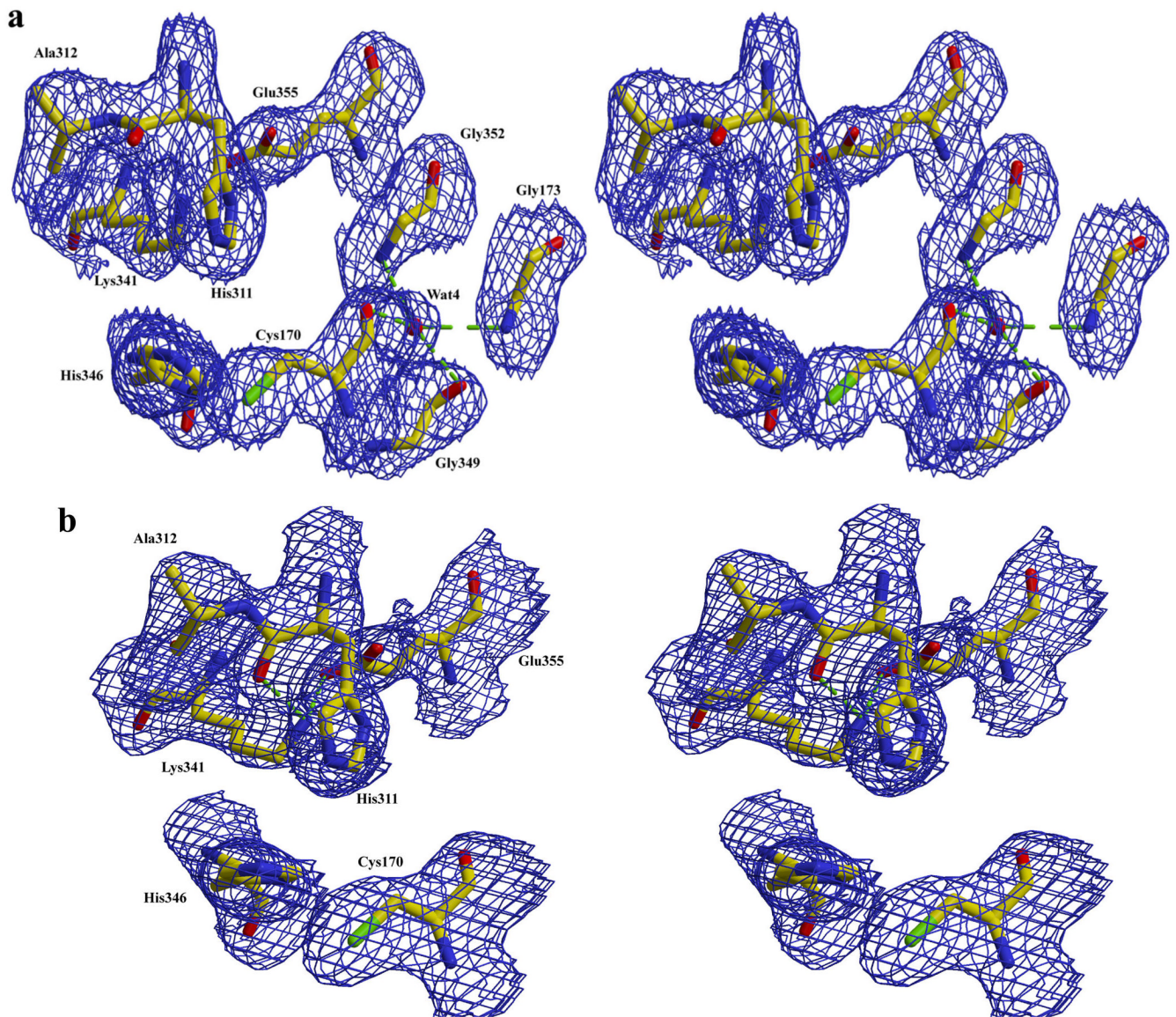


Figure 3.
 a) active site in subunit A of *mtKasB*. For clarity some of the residues that hydrogen bond with Wat4 and described in the text are not shown. b) active site in subunit B of *mtKasB*. In both a and b electron density contoured at 1.0σ level is shown in blue.

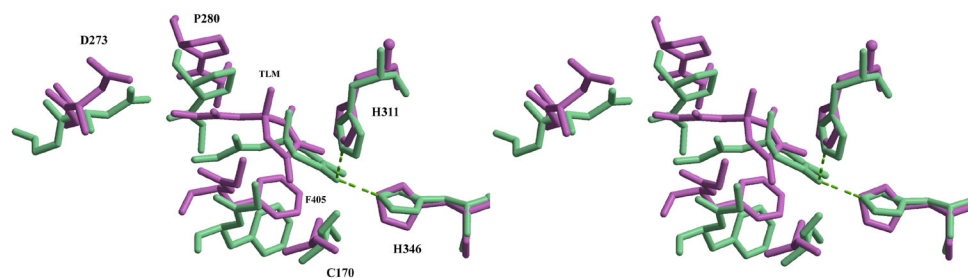


Figure 4. Superposition of TLM binding sites in *ecFabB*-TLM complex (1FJ4, green) and *mtKasB*-TLM model (magenta). The green dotted lines indicate interactions of TLM O2 with active site histidines in *ecFabB*-TLM complex.

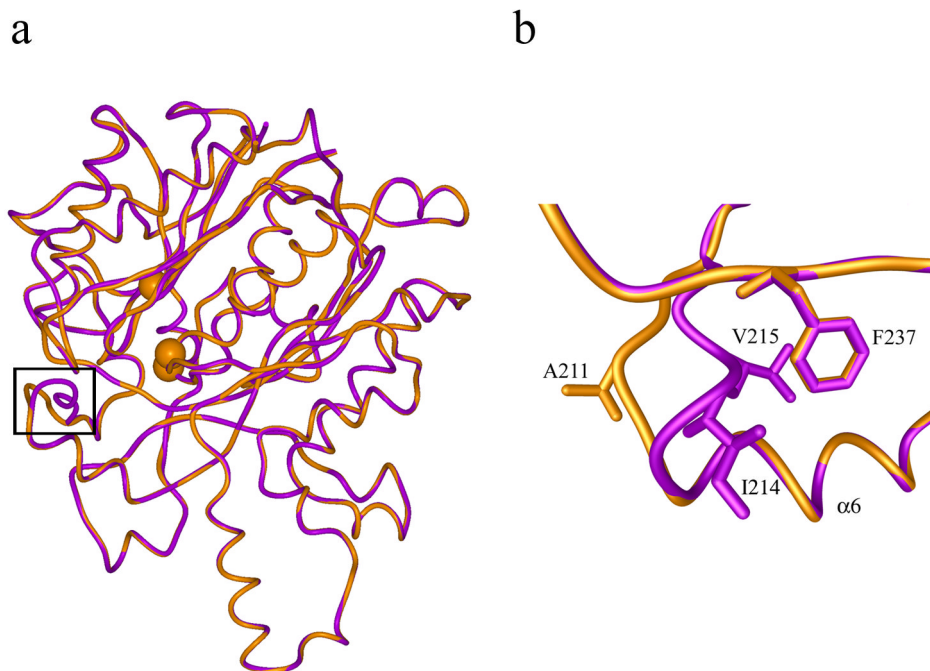


Figure 5.

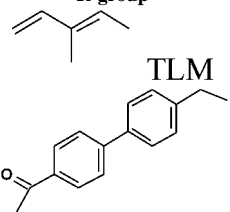
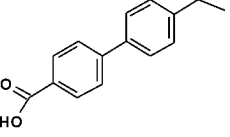
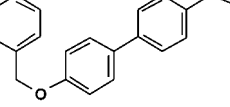
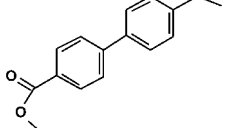
a) Superposition of *mtKasA* model (gold) and crystal structure of *mtKasB* (magenta). The structures are shown in worm representation. The $C\alpha$ atoms of the active site residues Cys170, His311 and His341 are shown as spheres. The black frame encloses the region of a loop at the entrance to the active site tunnel where the structures are different. b) A magnified view of the region shown in the black frame in a) representing the difference in the structure of the loop between *mtKasA* and *mtKasB*. The residues of this loop that are different between the two structures are labeled. This loop region follows the helix α_6 .

Table 1Data collection and refinement statistics for *mtKasB* structure determination

Data collection:	
Space group	R3
Cell dimensions (a, b, c in Å, α°, β°, γ°)	198.7, 198.7, 71.8, 90, 90, 120
Resolution (Å)	50-2.39
Completeness % (last shell)	98.6 (88.4)
I/σ(I) (last shell)	31.7 (2.5)
No. of total reflections	230006
No. of unique reflections	41266
R _{sym} % (last shell)	5.3 (43.1)
Refinement:	
Resolution (Å)	50-2.4
No. of reflections in test set	1911
No. of reflections in working set	35874
No. of protein molecules in asu	2
No. of protein atoms in asu	6192
No. of water molecules in asu	229
Twinned R-factor (%)	23.6
Twinned R _{free} factor (%)	18.1
RMS deviations:	
Bond lengths (Å)	0.007
Bond angles (°)	1.15
Average B-factors (Å ²):	
Main chain	53.9
Side chain and waters	54.4
RMS B main chain	0.75
RMS B side chain	0.89

$R_{sym} = \sum |I - \langle I \rangle| / \sum I$, where $\langle I \rangle$ is the average intensity over symmetry equivalents.

Table 2
Structures and IC₅₀ values against *mtKasA* of TLM analogues 1-4

No.	R-group	IC ₅₀ (μM)
1	 TLM	63
2		86
3		46
4		66